Journal of the Chinese Society of Mechanical Engineers, Vol.47, No.4, pp363~372 (2026)

Optimization of Surface Texture for Friction Performance in Continuous Rotary Electro-Hydraulic Servo Motor Friction Pairs

Xiao-Jing Wang*, Sun-Meng Yuan** ,Zi-Qin Peng***and Hui Meng***

Keywords：Surface texture, Continuous rotary motor, Oil film pressure, Friction performance.

ABSTRACT

The objective of this study is to investigate the effect of surface texture on the friction performance of continuous rotary motor friction pairs. A simplified model of the gap flow field between the motor blade and stator friction pair was constructed. Simulations of fluid models with varying textures were conducted using FLUENT software to analyze the relationship between the maximum positive pressure of the oil film, load-carrying capacity, and friction coefficient. Based on the simulation results, an optimal texture was machined onto specimens for friction testing. The influence of surface texture on friction performance was assessed by comparing friction coefficients between textured and smooth surfaces at different speeds and loads. The results demonstrate that the designed surface texture significantly enhances the friction performance of motor friction pairs.

INTRODUCTION

The continuous rotary electro-hydraulic servo motor, crucial for flight attitude simulation, demands a high-performance system with ultra-low speed, rapid response, and precise control (Yan, 2013; Li, 2014). Traditional research focusing on control strategies does not adequately address the core friction issues. Surface texturing, a globally emerging tribological innovation, significantly enhances the friction characteristics of these motors (Yang et al., 2021; Yin et al., 2021; Hu et al., 2019; Zhong et al., 2020). Therefore, investigating its impact on the performance of friction pairs is crucial for enhancing overall performance.

Extensive studies have demonstrated that well-designed and optimized surface textures can significantly reduce friction and wear, while enhancing oil film load capacity, system stability, and dynamic performance. In a similar manner, Janssen et al. (2017) utilized picosecond laser machining to create surface textures that improved lubrication. Scaraggi et al. (2013) demonstrated that the presence of pits on aluminum alloys led to a reduction in the friction coefficient by almost 50%. In contrast, traditional grooves were found to increase friction by 80–100% under mixed lubrication conditions. As Henry et al. (2015) emphasized, the load-dependence of texture density is a key consideration. In situations where low-density textures are employed, they are shown to be preferable under light loads. Conversely, high-density textures are demonstrated to perform better under heavy loads. Arsland et al. (2015) found that on DLC coatings, texture sizes within 100 μm delivered optimal friction reduction, while sizes beyond 300 μm showed diminished performance.

Texture geometry and placement are critical design parameters influencing lubrication. Inspired by the textures of hogweed surfaces, Gao et al. (2025) proposed a pillar-lunar composite texture and found that a non-dimensional depth of 0.8 μm yielded the best load capacity, with isotropic uniform arrangements outperforming other patterns. Zhou et al. (2025) provided a summary of the optimal geometry ranges that were observed under various lubrication regimes. For gas lubrication, a depth-to-diameter ratio of 0.005–0.01 and an area ratio of 10%–50% were recommended. For liquid lubrication, the preferred

Paper Received September, 2024. Revised June, 2025. Accepted July, 2025. Author for Correspondence: Xiao-Jing Wang.

* *Professor, School of Mechanical-Electronic and Vehicle Engineering, Beijing University of Civil Engineering and Architecture, Beijing 100044, China.*

** *Graduate Student, School of Mechanical-Electronic and Vehicle Engineering, Beijing University of Civil Engineering and Architecture, Beijing 100044, China.*

*** *Graduate Student, School of Mechanical and Power Engineering, Harbin University of Science and Technology, Heilongjiang, Harbin 150080, China.*

J. CSME Vol.47, No.4 (2026)
10.29979/JCSME.202608_47(4).0006

ratios were 0.01–0.02 and 30%–60%. These findings provide a valuable reference point for the design of textures on piston rings and seals. From a structural optimization perspective, Nie et al. (2022) recommended placing textures in the converging zone of sliding bearings to enhance oil film pressure, while diverging zones impaired performance. Niu et al. (2021) implemented partial texturing with 60% coverage and 4.9% area ratio on bearing surfaces, thereby achieving a 45.8% reduction in peak vibration amplitude at 9000 rpm. This, in turn, resulted in improved dynamic stiffness and operational stability.

In hydraulic systems, surface texturing has been shown to have significant advantages. As posited by Wei et al. (2019), the application of micro-dimples on plungers and barrels has been demonstrated to reduce friction and wear under conditions of oil/water lubrication. In the study by Chen et al. (2019), multi-scale textures on axial piston pumps were optimized using NSGA-II. The resultant enhancement in performance was evidenced by a reduction in friction torque of 8.2% and leakage of 9.9%. As Ma et al. (2019) found, the presence of textures on swash plate surfaces resulted in the thickening of oil film and a reduction in friction. As demonstrated by Liu (2019), texture-based friction reduction in motors operating in seawater has been confirmed. As demonstrated by Zhang et al. (2021), the combination of textures with boronizing resulted in a 47.6% reduction in leakage and an enhancement in wear resistance.

In order to optimize multiple parameters, orthogonal experimental methods are utilized extensively. Wang et al. (2022) conducted a study to ascertain the effects of blade extension ratio, forewing curvature, and airfoil gap on hydrodynamic performance. To this end, orthogonal tests were used. Bao et al. (2024) applied an orthogonal design to optimize water jacket extension for the purpose of enhancing cooling. Feng et al. (2024) utilized the Box–Behnken method to enhance the efficacy of garlic seed metering, thereby minimizing seed damage. These techniques offer effective frameworks for the optimization of texture parameters.

In the present study, the friction between the blade and stator of a continuous rotary electro-hydraulic servo motor is investigated, and the effects of the shape, size, depth, and area rate of the surface texture on the friction performance are analyzed. Surface textures with different morphological and geometrical parameters were optimized by one-way and orthogonal tests. The optimal surface texture parameters for the friction components of motor blades and stators were identified and evaluated on specimens. The impact of surface texture on friction performance was assessed by comparing the friction coefficients of textured surfaces with those of smooth surfaces at varying speeds and loads.

CONTINUOUS ROTARY ELECTRO-HYDRAULIC SERVO MOTOR STRUCTURE AND ITS SURFACE TEXTURED FLUID MODELLING

Fig. 1 depicts the internal structure and physical diagram of the continuous rotary electro-hydraulic servo motor, which comprises blades, stator, rotor, oil distribution disc, end cap, and sleeve. The primary friction contacts occur at the top of the blades and the stator's inner surface, between the blades and blade grooves, and at the end faces of the blades and rotor against the oil distribution disc.

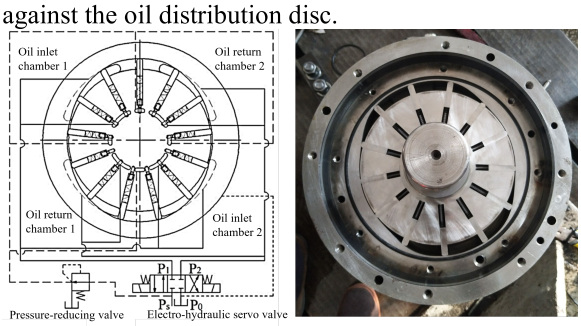

Fig. 1. Internal structure of continuous rotary electro-hydraulic servo motor.

Establishment of a geometrical model of surface weaving and simplification methods

As shown by the blade structure in Fig. 2, in a c continuous rotary electro-hydraulic servo motor, the curvature of the stator is significantly larger than the thickness of the gap oil film, so the contact surface between the blade and the stator is approximately planar. When the motor is running, blade motionis considered planar due to minimal curvature effects. By modeling the flow field of a single surface texture with appropriate boundary conditions, this single texture flow field model can be used to effectively analyze the effect of a single texture on the performance of the friction pair. A simplified flow of the flow field is shown in Fig. 3.

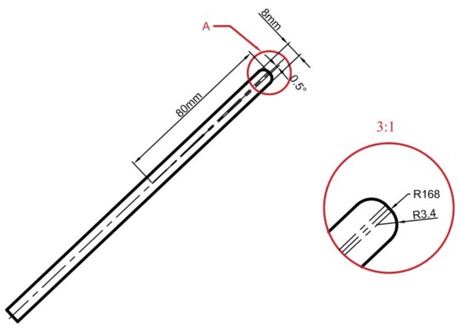

Fig. 2. Motor vane structure.

Fig. 3. Simplified flow field model.

Fig. 4 shows a schematic cross-section of five types of fabrics, namely, cylindrical surface fabrics, spherical surface fabrics, conical surface fabrics, square surface fabrics, and parabolic surface fabrics, which are designed on the blades of a continuous rotary electro-hydraulic servo motor.

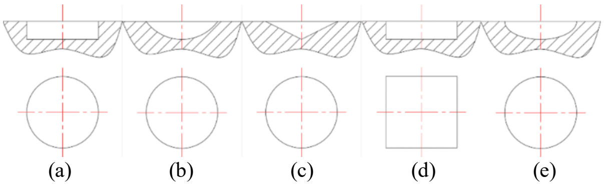

Fig. 4. Schematic cross-sections of surface weaves of different morphologies: (a) cylindrical, (b) spherical, (c) conical, (d) square, (e) parabolic.

Computational pre-treatment for surface textured fluid simulation

In the simulation, five fluid models with varying surface textures were designed using SolidWorks. Prior to numerical calculations, mesh delineation was performed using ICEM-CFD. For instance, the cylindrical surface texture was meshed using a structured grid, as depicted in Fig. 5, which show the meshing of the cylindrical texture model and the mesh quality, respectively. The mesh consisted of approximately 96,000 meshes.

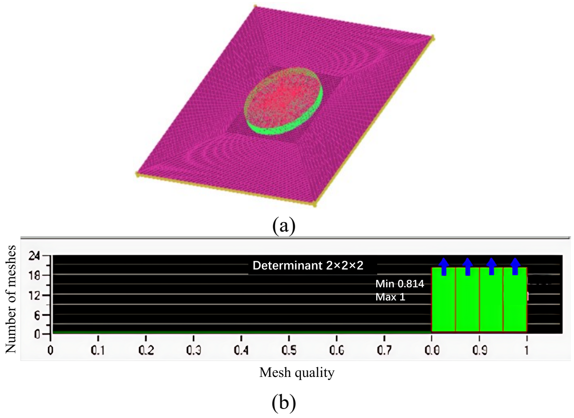

Fig. 5. (a) Mesh partitioning and (b) mesh quality for fluid models with different morphological textures.

Fig. 6 depicts the surface texture simulation model utilized for the friction vice. The side length of the square unit is determined by the texture size and area rate. In the model, the upper wall represents the moving surface, while the lower wall is fixed. The rotational speed of the motor blade, set at 10 r/min, translates to a linear speed of 0.12 m/s for the upper wall, which moves in a specified direction.

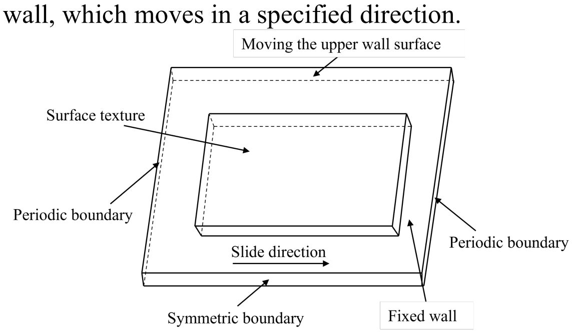

Fig. 6. Simulation model for surface texture of friction pairs.

The meshed fluid model is imported into Fluent, where the surface weaving fluid model and boundary conditions are established. The model employs the Mixture model for multi-phase flow and the default Schnerr-Sauer cavitation model in Fluent. Calculations are performed using the Coupled algorithm and discretized with the First Order Upwind algorithm, with iterations set to 1000 and other settings at default values. Table 1 lists the relevant calculation parameters.

Table 1. Related calculation parameters

Calculated parameter	Numerical value
Barometric pressure p_0/Pa	101325
Cavitation pressure p_c/Pa	30000
Fluid viscosity η/(Pa·s)	0.0288
Fluid density ρ/(kg·m^3)	870
Upper wall travelling speed U/(m·s^{-1})	0.12

Table 2. Software and experimental configurations used in simulation and testing

Category	Item	Specification
Modeling & Simulation	Modeling software	SolidWorks 2021
	Meshing software	ANSYS ICEM-CFD 2022 R1, structured mesh, ~96,000 elements
	Simulation software	ANSYS Fluent 2022 R1
	Simulation model	Mixture multiphase model + Schnerr–Sauer cavitation model
	Solver settings	Coupled algorithm, First Order Upwind, 1000 iterations
Experimental Setup	Test apparatus	MWF-10 reciprocating friction and wear tester
	Upper specimen material	W18Cr4V high-speed steel, Ra 0.4
	Lower specimen material	38CrMoAl nitriding steel, Ra 0.8
	Lubricant	No. 32 hydraulic oil (η = 0.0288 Pa·s, ρ = 870 kg/m³, p_c =0.5-5kPa)
	Texture fabrication method	Micro-electrochemical machining
	Test parameters	Frequency: 0.5–1.5 Hz; Load: 2–5 MPa; Duration: 600 s per test
	Environmental conditions	Temperature: 25 ± 1 °C; Ambient pressure: 101325 Pa

DISCUSSION AND ANALYSIS OF NUMERICAL CALCULATION RESULTS

Typical pressure distribution on the wall of the oil film

When surfaces have a weave, the oil passing through them will create high-pressure and low-pressure areas. Whether or not the cavitation effect is considered, it will have a significant impact on the pressure distribution of the moving wall. The pressure distribution of the moving wall with or without considering the cavitation effect is illustrated in Fig. 7.

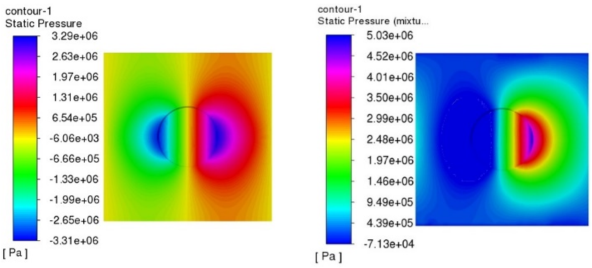

(a) (b)

Fig. 7. Moving wall pressure distribution: (a) Cavitation not considered and (b) Consider cavitation.

Influence of surface texture on the oil film pressure field in the friction gap and its optimization

Parameter Selection Basis for Surface Texture Design

The texture parameters – area ratio S_p, feature size r_p or a, and depth h_p – were selected based on a review of the extant literature, preliminary simulations, and fabrication limits. The area ratio (10%–50%) and feature sizes (50–250 μm radius or 88–443 μm side length) reflect common ranges used in tribological studies (Nie et al., 2022). Depths between 10–30 μm were found to ensure both manufacturability and effective pressure generation (Arslan et al., 2015).

Since leakage is a critical concern in electro-hydraulic servo motor, parameters were constrained to minimize flow loss. According to the principles of lubrication theory, the leakage volume Q through textured gaps can be estimated by the following equation:

$$Q \propto \frac{S_p \cdot h_p^3}{\eta \cdot L} \tag{1}$$

Where Q is the leakage volume per unit time, S_p is the area rate of the weave, h_p is the depth of the weave, η is the fluid viscosity, and L is the effective length of the oil film in the direction of flow. It can be seen that the increase in the area rate and depth will exacerbate the leakage risk with a cubic trend, provided that other parameters remain constant. Therefore, in this study, S_p =10% -50% and h_p =10-30 μm were set to minimize this effect.

Calculated results of surface texture simulation with different area ratio

Firstly, the effect of the area rate of the surface texture on the gap oil film pressure is investigated, and the oil film pressure distribution under different texture area rates is solved by changing the size of the texture area rate. The geometrical parameters of cylindrical, square, spherical, conical, and parabolic surface textures with different area rates are shown in Table 3.

Table 3. Geometric parameters of different texture models with different area ratios

Geometric parameter / Type of structure	h_0 (μm)	S_p (%)	r_p/ a (μm)	h_p (μm)
Cylindrical	10	10/20/30/40/50	200	10
Square	10	10/20/30/40/50	354.5	10
Ball-shaped	10	10/20/30/40/50	200	10
Conic	10	10/20/30/40/50	200	10
Parabolic shape	10	10/20/30/40/50	200	10

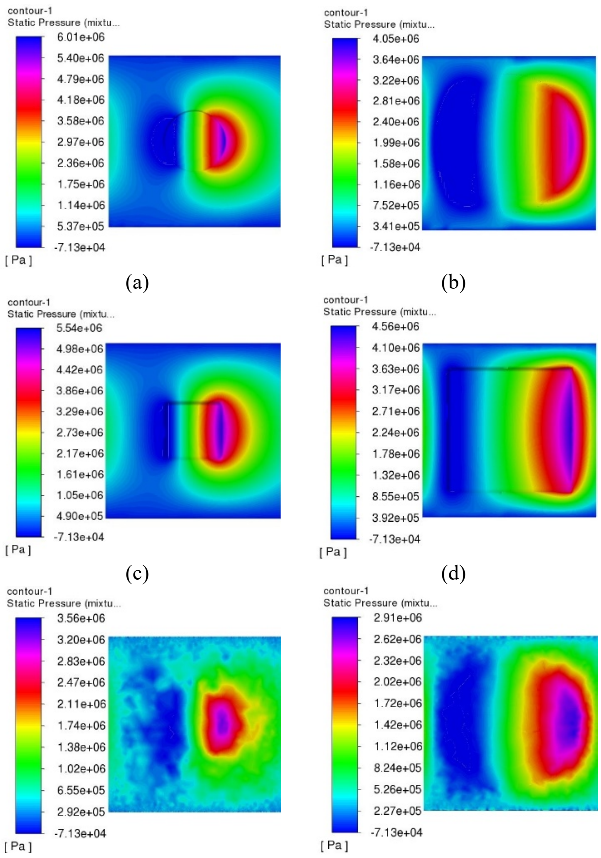

(a) (b) (c) (d) (e) (f)

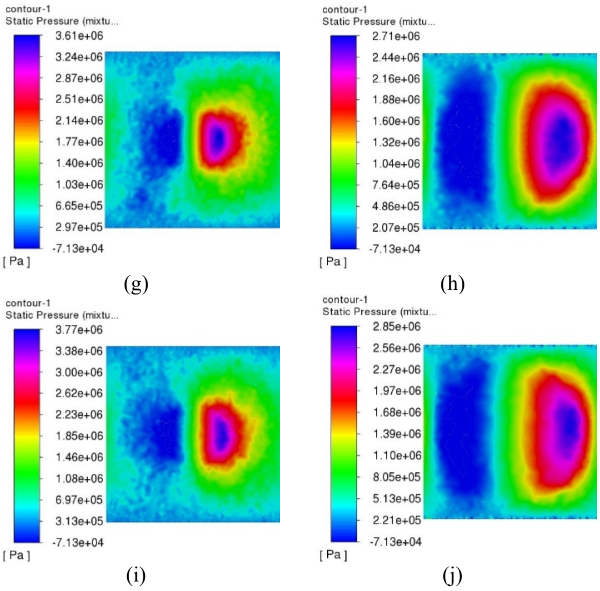

Fig. 8. Pressure distribution of texture under different area ratios: (a) Cylindrical S_p=10; (b) Cylindrical S_p=50; (c) Square S_p=10; (d) Square S_p=50; (e) Spherical S_p=10; (f) Spherical S_p=50; (g) Conical S_p=10; (h) Conical S_p=50; (i) Parabolic S_p=10; (j) Parabolic S_p=50.

Due to space constraints, only the simulation results corresponding to textured area ratios of 10% and 50% are presented in this paper, as illustrated in Fig.8. According to Fig.8, cylindrical, square, spherical, conical, and parabolic weaves all exhibit the highest positive pressure of the oil film at an area rate of 10% of the weave before decreasing with a higher area rate. Therefore, a 10% area rate was selected for subsequent study.

The oil film load carrying capacity can be obtained by integrating the pressure on the moving upper surface over a unit area, and the load carrying capacity equation is as follows.

$$W = \iint p(x, y)dxdy \tag{2}$$

Where, W is the oil film bearing capacity in N; $p\ (x, y)$ is the pressure distribution on the oil film.

The coefficient of friction can be obtained by extracting the friction force on the moving upper surface and quoting it with the oil film carrying capacity.

The shear force on the upper surface can be integrated over the unit area to obtain the friction on the moving wall. The resulting friction equation is then determined.

$$F_x = \iint \tau dxdy \tag{3}$$

Where, F_x is the tangential friction force in N; τ is the shear force N on the wall.

The friction coefficient f is therefore as follows.

$$f = \frac{F_x}{W} \tag{4}$$

Fig. 9 illustrates the relationship between the maximum pressure, oil film carrying capacity and friction coefficient of the upper moving surface and the weave area ratio for a cylindrical weave as an example. The analysis shows that as the weave area ratio increases, the maximum pressure and oil film carrying capacity decrease, while the coefficient of friction increases. Therefore, the maximum pressure on the upper surface can be used as an indicator of the performance of the friction pair.

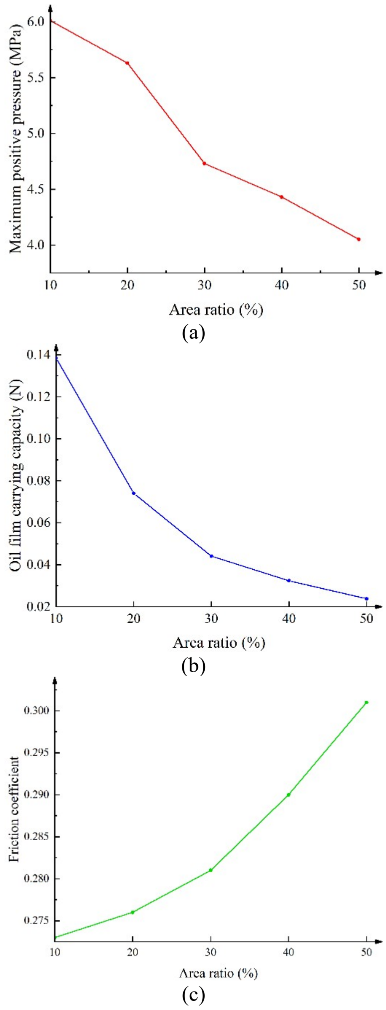

Fig. 9. The relationship between (a) maximum positive pressure, (b) oil film carrying capacity, (c) friction coefficient, and texture area ratio in motion.

Simulation results of surface texture for different texture sizes

In order to analyze the effect of the weave size on the gap oil film pressure, the film thickness, area ratio, and depth of the weave were kept constant, and the dimensions of the surface weaving unit were changed, in which the radius variables of cylindrical, spherical, conical, and parabolic shapes were set to be

50, 100, 150, 200, and 250μm, and the side lengths of the squares were set to be 88, 177, 265, 354, and 443μm. The oil film pressure distributions of different weaves at different sizes were simulated in Fluent and analyzed to obtain the maximum oil film pressure plot with contact surface area as x-axis as shown in Fig. 10.

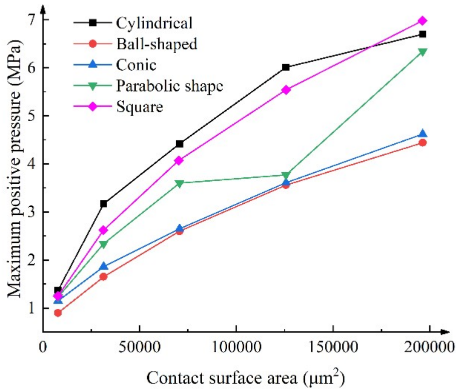

Fig. 10. Maximum pressure distribution for different textures at different sizes

Fig. 10 demonstrates that as the dimensions of cylindrical, square, spherical, conical, and parabolic weaves increase, the maximum positive pressure of the oil film also increases. The optimal weave radius of 250μm for cylindrical, spherical, conical, and parabolic textures, along with the square weave side length of 443μm, are selected to provide the best weave radii for subsequent analysis.

Calculated results of surface texture simulation with different texture depths

After determining the other parameters of each braid, the effect of surface braiding depth as a variable on the gap oil film pressure was investigated, and the surface braiding depths of cylindrical, square, spherical, conical, and parabolic shapes were set to 10, 15, 20, 25, and 30μm, respectively, and the oil film pressure distributions of the different textures at different depths were obtained by simulation in Fluent, and the analysis yielded the maximum oil film pressure plots with the depth as the x-axis as shown in Fig. 11.

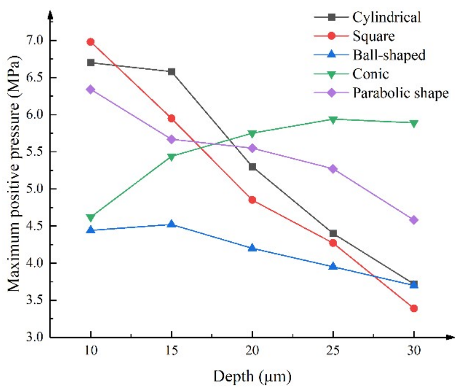

Fig. 11. Maximum pressure distribution for different textures at different depths.

According to the optimization results of the one-way test, the maximum positive pressure of the oil film is the greatest at a depth of 10 μm for cylindrical and square weave, 15 μm for spherical weave, 25 μm for conical weave, and 10 μm for parabolic weave, which has the greatest influence on the friction performance of the friction pair.

After the above CFD simulation analysis and comparison, it is found that the maximum positive pressure of the oil film is the largest when the area ratio of the square weave is 10%, the weave side length is 443 μm, and the weave depth is 10 μm, and the maximum positive pressure value is 6.98 MPa.

Simulation results of orthogonal test programme

Orthogonal test is an effective multifactorial experimental design method for seeking the optimal combination of factor levels, which can quickly obtain the best combination and facilitate the processing of experimental data, the factor level table is shown in Table 4.

Table 4. Factor level table

Level	Area ratio (%) A	Radius (μm) B	Depths (μm) C	Textural morphology D
1	10	50	10	Cylindrical
2	20	100	15	Conic
3	30	150	20	Parabolic shape
4	40	200	25	Ball-shaped
5	50	250	30	Square

Simulation analysis was carried out according to the orthogonal test programme and the table of polar analysis obtained from the simulation according to the orthogonal test programme is shown in Table 5.

Table 5. Range Analysis Table

	A	B	C	D
K1	15.36	6.59	13.15	13.17
K2	13.29	9.85	14.56	13.64
K3	14.49	13.70	14.32	14.95
K4	13.74	16.40	13.76	14.85
K5	11.17	21.45	12.20	11.38
k1	3.07	1.32	2.63	2.63
k2	2.66	1.97	2.91	2.73
k3	2.90	2.74	2.86	2.99
k4	2.75	3.28	2.75	2.97
k5	2.23	4.29	2.44	2.28
Extremely poor (R)	0.84	2.97	0.47	0.71
Order of priority	B>A>D>C			
Excellent level	A1	B5	C2	D3
Superior combination	A1B5C2D3			

The extreme variance analysis revealed that the weave size has the greatest impact on the maximum positive pressure of the oil film, followed by the area rate and morphology, with depth having the least impact. Despite the preferred combination yielding a maximum pressure of 5.67 MPa, it was below the optimal 6.98 MPa from the one-way test. Consequently, a square weave with a 10% area rate, an edge length of 443 μm, and a depth of 10 μm was selected for further investigation.

EXPERIMENTAL STUDY ON THE EFFECT OF SURFACE TEXTURE ON THE FRICTION PERFORMANCE OF FRICTION SUBSTITUTES

Test methods

The study utilized tungsten high-speed steel (W18Cr4V) for the blade specimens, achieving a friction surface roughness of Ra0.4 and a general surface roughness of Ra3.2. Advanced nitriding steel (38CrMoAl) was chosen for the stator specimens, with a friction surface roughness of Ra0.8 and a general surface roughness of Ra6.3. Due to considerations of precision and cost, the microelectrolysis method was employed to texture the blade's friction surface. The resulting processed specimen is depicted in Fig. 12.

Fig. 12. Friction specimen after processing

At room temperature (25 ± 1 °C) and atmospheric pressure (p_0= 101325 Pa), an equal volume of No. 32 hydraulic fluid (viscosity η = 0.0245–0.0303 Pa·s, density ρ = 840–870 kg/m³, cavitation pressure p_e =0.5-5kPa) was first added to a stainless-steel sample container. The friction test was conducted using the MWF-10 reciprocating friction and wear tester, with the loading force set and the servo motor started to initiate the reciprocating friction movement, the system composition shown in Fig. 13. During the test, No. 32 hydraulic oil was employed for lubrication, as it is also the working fluid used in the actual operation of the rotary electro-hydraulic servo motor, thereby ensuring that the test conditions are representative of real-world operating conditions. The load and speed were adjusted as needed. The sampling time for each test was set to 10 minutes. The friction coefficient was recorded by the data acquisition system, and the relevant test procedures are detailed in Table 6.

In the simulation, the physical properties of No. 32 hydraulic oil were also incorporated to ensure consistency with the experimental conditions. Notably, the cavitation pressure was set to 30,000 Pa, which exceeds the actual value of the oil (0.5–5 kPa), to enhance numerical stability and ensure model convergence, especially under extreme operating conditions. This adjustment maintains consistency with physical trends while preventing non-physical divergence in low-pressure regions.

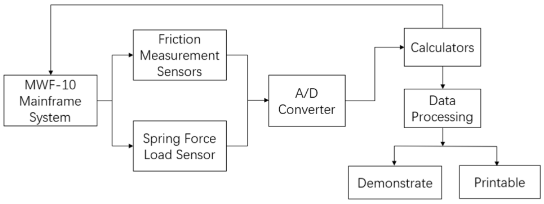

Fig.13. Composition diagram of friction and wear test bench.

Table 6. Friction test plan

Experiment number	Friction substitutes (Upper Specimen - Lower Specimen)	Reciprocating frequency (Hz)	Pressure load (MPa)	Experimental time (s)
1	Woven - Smooth	0.5	4	600
2	Smooth - Smooth	0.5	4	600
3	Woven - Smooth	1	4	600
4	Smooth - Smooth	1	4	600
5	Woven - Smooth	1.5	4	600
6	Smooth - Smooth	1.5	4	600
7	Woven - Smooth	1.5	2	600
8	Smooth - Smooth	1.5	2	600
9	Woven - Smooth	1.5	3	600
10	Smooth - Smooth	1.5	3	600
11	Woven - Smooth	1.5	5	600
12	Smooth - Smooth	1.5	5	600

Influence of surface texture on the friction performance of friction substitutes

Effect of friction properties at different speeds

(a) (b) (c)

(d) (e) (f)

Fig. 14. Macroscopic morphology of the sample after texture and smooth friction pair friction test: (a) 0.5Hz texture friction pair specimen; (b) 1Hz texture friction pair specimen; (c) 1.5Hz texture friction pair specimen; (d) 0.5Hz smooth friction pair specimen; (e) 1Hz smooth friction pair specimen; (f) 1.5Hz smooth friction pair specimen.

The test pressure load on the specimen was 4MPa. Fig. 14 (a)-(f) illustrates that the abrasion marks on the lower specimen's friction surface deepened with increasing reciprocation frequency and were notably deeper under the smooth friction subset compared to the textured sub-set.

Fig. 15 presents the friction coefficient as a function of reciprocating frequency for both textured and smooth specimens. The textured surface consistently demonstrates lower friction across all test conditions, with reductions of 9.67%, 9.62%, and 6.5% at 0.5 Hz, 1.0 Hz, and 1.5 Hz, respectively. Averaging a reduction of 8.6%, these results confirm the efficacy of surface texturing in reducing friction, particularly under low-to-moderate frequency regimes where boundary lubrication dominates.

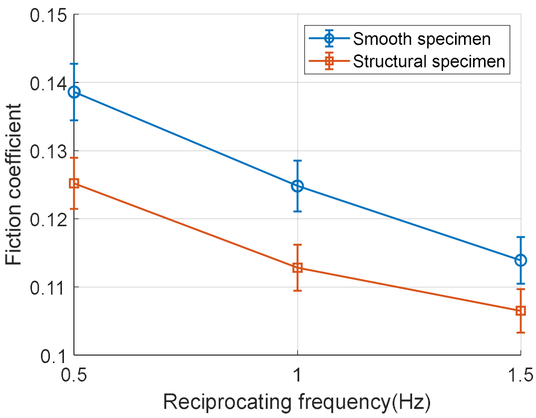

Fig. 15. Relationship between texture and smooth friction pair friction coefficient and velocity.

Effect of friction performance under different loads

(a) (b) (c)

(d) (e) (f)

Fig. 16. Macroscopic morphology of the sample after texture and smooth friction pair friction test: (a) Specimen under 2MPa weave friction pair; (b) Specimen under 3MPa weave friction pair; (c) Specimen under 5MPa weave friction pair; (d) Specimen under 2MPa smooth friction; (e) Specimen under 3MPa smooth friction; (f) Specimen under 5MPa smooth friction.

As shown in Fig. 16, after the friction test was conducted at a reciprocating frequency of 1.5 Hz, the surface of the specimens showed obvious differences in wear morphology. As the load was increased from 2 MPa to 5 MPa, the overall wear area of the specimens gradually increased, indicating that the rising load exacerbated the interaction between the material surfaces. However, the depth and sharpness of the wear marks decreased, which is presumed to be due to the uniformity of wear at higher loads. Further comparison of the weave friction pair and smooth friction pair specimens reveals that the wear degree of the weave surface is significantly lower than that of the smooth surface under the same load, which indicates that the weave structure can effectively disperse the contact stresses, reduce the local wear, and improve the wear resistance of the friction pair.

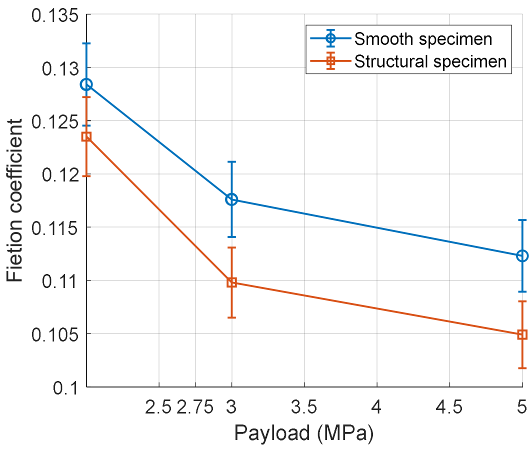

Fig. 17. Relationship between texture and smooth friction pair friction coefficient and load.

As illustrated in the fig. 17, the friction coefficient of both smooth and textural specimens declines as the load increases from 2 MPa to 5 MPa. The textured surface consistently demonstrates superior tribological performance, with friction reductions of 3.82%, 6.63%, and 6.77% at 2, 3, and 5 MPa, respectively. On average, the friction coefficient is reduced by approximately 5.74%, thereby confirming the efficacy of the texture in minimizing frictional resistance under elevated loading conditions.

CONCLUSION

1. A one-factor test scheme and an orthogonal test scheme were designed with the maximum positive pressure on the oil film surface as the target, and the flow field model of the weave under different morphology and geometrical parameters was simulated using FLUENT software, and the weave applied to the friction vice of the motor was obtained to be a square weave with an area rate of 10%, a side length of 443 μm, and a depth of 10 μm;
2. Extreme variance analysis was carried out by orthogonal tests, and it was found that the main order of influence on the maximum positive pressure of the oil film was the size of the weave, the rate of area, the morphology and the depth;
3. The MWF-10 reciprocating friction and wear testing machine was utilized to assess the friction performance of weave friction pairs under oil lubrication, with a comparison made to smooth friction pairs. The findings indicate a decrease in the friction coefficient with an increase in reciprocating frequency and load. On average, the textile friction pair exhibited an 8.6% reduction in friction at varying frequencies and a 5.74% reduction at different loads, demonstrating superior frictional and wear performance compared to the smooth friction pair.

ACKNOWLEDGMENT

Financial support for this work was provided by National Natural Science Foundation of China (No: 52375037), Distinguished Youth Fund Project of Beijing University of Civil Engineering and Architecture (No: GDRC20220801), Master's Innovation Project of Beijing University of Civil Engineering and Architecture (No: PG2024142) and Breeding program Funding of Beijing University of Civil Engineering and Architecture (No: X24026)

REFERENCES

Yan, W.P., "Research on Key Seal and Component of Swing Electro-Hydraulic Servo Motor Applied to Simulator," Master's thesis, Harbin Institute of Technology, Harbin (2013)

Li, Z., "Research on Control Methods of High Precision Turntable," Master's thesis, Xidian University, Xi'an (2014)

Yang, F.S., Lin, W., Duan, J.S., "Research on Surface Micro-Texture Technology of Wedm," *Machine Tool & Hydraulics* Vol. 49, No. 6, pp. 27–31 (2021)

Yin, H.Z., W.G., C., Li, R.B., "Friction Performance of Wedge-Shaped Texture on the Surface of 3d Printed Abs Materials," *China Surface Engineering* Vol. 34, No. 4, pp. 158–166 (2021)

Hu, D., Guo, Z.W., Xie, X., "Effect of Spherical-Convex Surface Texture on Tribological Performance of Water-Lubricated Bearing," *Tribology International* Vol. 134, pp. 341–351 (2019)

Zhong, B., Xing, Z.G., Wang, H.D., "Research Progress on the Tribological Properties of Textured Surfaces," *Materials Reports* Vol. 34, No. 23, pp. 23171–23178 (2020)

Janssen, A., Pinedo, B., Igartua, A., "Study on Friction and Wear Reducing Surface Micro-Structures for a Positive Displacement Pump Handling Highly Abrasive Shale Oil," *Tribology International* Vol. 107, pp. 1–9 (2017)

Scaraggi, M., Mezzapesa, P.F., Carbone, G., "Friction Properties of Lubricated Laser-MicroTextured-Surfaces: An Experimental Study from Boundary- to Hydrodynamic-Lubrication," *Tribology Letters* Vol. 49, No. 1, pp. 117–125 (2013)

Henry, Y., Bouyer, J., Fillon, M., "An Experimental Analysis of the Hydrodynamic Contribution of Textured Thrust Bearings During Steady-State Operation: a Comparison with the Untextured Parallel Surface Conffguration," *Proceedings of the Institution of Mechanical Engineers, Part J: Journal of Engineering Tribology* Vol. 229, No. 4, pp. 362–375 (2015)

Arslan, A., Masjuki, H.H., Varman, M., "Effects of Texture Diameter and Depth on the Tribological Performance of DLC Coating Under Lubricated Sliding Condition," *Applied Surface Science* Vol. 356, pp.1135–1149 (2015)

Gao, C., Ding, X.H., Zhang, H., "Design of the Lubricating Biomimetic Texture Based on the Wax Area of Nepenthes Alata ," *Tribology* pp. 1-17 (2025)

Zhou, H., Yang, H.Y., Zhu, T.Y., "Simulation Analysis and Load-carrying Capacity Map of Dimple Textures under Gas and Liquid Lubrication Conditions ," *Tribology* pp. 1-16 (2025)

Nie, T., Yang, K., Zhou, L., "CFD Analysis of Load Capacity of Journal Bearing with Surface Texture," *Energy Reports* Vol. 8, No. S7, pp. 327–334 (2022)

Niu, Y.S., Hao, X.G., Xia, A.N., "Effects of Textured Surfaces on the Properties of Hydrodynamic

Bearing," *The International Journal of Advanced Manufacturing Technology* Vol. 118, No. 5–6, pp. 1–8 (2021)

Wei, S.B., Shang, H.F., Liao, C.L., "Tribology Performance of Surface Texturing Plunger," *Biomimetics* Vol. 4, No. 3, pp. 54 (2019)

Chen, Y., Zhang, J.H., Xu, B., "Multi-Objective Optimization of Micron-Scale Surface Textures for the Cylinder/Valve Plate Interface in Axial Piston Pumps," *Tribology International* Vol. 138, pp. 316–329 (2019)

Ma, X., Wang, J.Q., Lu, X., "Piston Surface Design to Improve the Lubrication Performance of a Swash Plate Pump," *Tribology International* Vol. 132, pp. 275–285 (2019)

Liu, J.C., "Lubrication Characteristic Simulation and Wear Test of Valve Port Pair of Seawater Motor with Bionic Non-Smooth Surface," Master's thesis, Yanshan University, Hebei (2019)

Zhang, D. Y., Li. Z.W., Wang. L.P., "Study on Tribological Properties of Boronized and Textured Composite Surface and Its Application on Camshaft Connecting-Rod Type Hydraulic Motor," *Wear*, pp. 482–483 (2021)

Wang, L., Zhang, X., Wan, R., "Optimization of the Hydrodynamic Performance of a Double-Vane Otter Board Based on Orthogonal Experiments," *Journal of Marine Science and Engineering* Vol. 10, No. 9, pp. 1177 (2022)

Bao, Y.Z., Lei, J.L., Li, W.X., "Research on Thermal Deformation of Cylinder Bore With Orthogonal Experiment Method of Aluminum Alloy Cylinder Block in Diesel Engine," *Applied Thermal Engineering* Vol. 245, pp. 122772 (2024)

Feng, D.H., Li, H., Qi, X.D., "Design and Laboratory Experiments of a Pneumatic Disc-Type Garlic Precision Seed-Metering Device," *AMER SOC Agricultural & Biological Engineers* Vol. 67, No. 2, pp. 451–460 (2024)